

Reduction of photobleaching and photodamage in single molecule detection: observing single actin monomer in skeletal myofibrils

Julian Borejdo

Priya Muthu

John Talent

Zygmunt Gryczynski

University of North Texas Health Science Center
Department of Molecular Biology and Immunology
Fort Worth, Texas 76107

Nils Calander

University of North Texas Health Science Center
Department of Molecular Biology and Immunology
Fort Worth, Texas
and

Chalmers University of Technology
Department of Microtechnology and Nanoscience
S-412 96 Göteborg, Sweden

Irina Akopova

University of North Texas Health Science Center
Department of Molecular Biology and Immunology
Fort Worth, Texas 76107

Tanya Shtoyko

University of Texas at Tyler
Department of Chemistry
Tyler, Texas 75799

Ignacy Gryczynski

University of North Texas Health Science Center
Department of Molecular Biology and Immunology
Fort Worth, Texas 76107
and

University of North Texas Health Science Center
Department of Cell Biology and Genetics
3500 Camp Bowie Boulevard
Fort Worth, Texas 76107

1 Introduction

Recently, it has become possible to study single protein molecules in a cell.^{1,2} The advantage of single molecule detection (SMD) is that it studies behavior of proteins in their native (crowded) environment, and avoids problems associated with averaging responses of an assembly of molecules with different kinetics. But the single molecule approach is complicated by photobleaching and cell damage, which arise because a sample must be illuminated with the intense laser beam to assure adequate signal-to-noise ratio (SNR).

In earlier work, we were able to decrease photobleaching and reduce photodamage by making measurements on glass

Abstract. Recent advances in detector technology make it possible to achieve single molecule detection (SMD) in a cell. SMD avoids complications associated with averaging signals from large assemblies and with diluting and disorganizing proteins. However, it requires that cells be illuminated with an intense laser beam, which causes photobleaching and cell damage. To reduce these effects, we study cells on coverslips coated with silver nanoparticle monolayers (NML). Muscle is used as an example. Actin is labeled with a low concentration of fluorescent phalloidin to assure that less than a single molecule in a sarcomere is fluorescent. On a glass substrate, the fluorescence of actin decays in a step-wise fashion, establishing a single molecule detection regime. Single molecules of actin in living muscle are visualized for the first time. NML coating decreases the fluorescence lifetime 17 times and enhances intensity ten times. As a result, fluorescence of muscle bleaches four to five times slower than on glass. Monolayers decrease photobleaching because they shorten the fluorescence lifetime, thus decreasing the time that a fluorophore spends in the excited state when it is vulnerable to oxygen attack. They decrease damage to cells because they enhance the electric field near the fluorophore, making it possible to illuminate samples with weaker light. © 2008 Society of Photo-Optical Instrumentation Engineers. [DOI: 10.1117/1.2938689]

Keywords: single molecule detection; nanoparticle monolayers; actin; photobleaching.

Paper 07430 received Oct. 19, 2007; accepted for publication Jan. 9, 2008; published online Jun. 20, 2008.

coated with nanoparticles known as surface island films (SIFs).³ SIFs are nanoparticles⁴⁻¹⁰ that can support confined charge density oscillations¹¹ called localized surface plasmon polariton (LSP) modes. Excitation of LSPs causes a strong enhancement of local electric fields and a substantial decrease of the fluorescence lifetime caused by the distance-dependent changes in radiative decay rates.¹² Specifically, the intensity of rhodamine fluorescence increased four to five fold, and its fluorescence lifetime decreased on average 23 fold. As a consequence, the rate of photobleaching of rhodamine actin in a myofibril placed on glass coverslips coated with SIF decreased approximately seven fold in comparison with photobleaching of myofibrils placed on uncoated coverslips. Recently, we showed that the enhancement could be even further

Address all correspondence to Julian Borejdo, Mol Biol, University of North Texas HSC, 3500 Camp Bowie Blvd, Fort Worth, TX 76107; Tel: +817-735-2106; Fax: 817-735-2118; E-mail: jboorejdo@hsc.unt.edu

increased when LSPs in nanoparticles were combined with propagating surface plasmons (PSPs) traveling in coverslips covered with a continuous film of noble metal. The interaction of these two kinds of plasmons with fluorophores in muscle caused more than a 200-fold increase of brightness.¹³

The price of the reduction of bleaching and photodamage was loss of optical resolution and nonuniformity of illumination, because SIF refracted exciting and fluorescent light. Moreover, nanoparticles were distributed randomly on the surface of a coverslip, and therefore reduction of photobleaching and photodamage was nonuniform. This prevented the use of SIF in single molecule detection, because maximal optical resolution is important in resolving single molecules. In studying cells, it is important to observe only a specific area [region of interest (ROI)], where interaction of interest occurs (e.g., cell nucleus). In the example used here—skeletal muscle myofibrils—actin and myosin filaments interact to produce contractile force in a narrow area known as the overlap zone (O-band). It spans the distance of 0.7 to 0.3 μm in resting length myofibrils,^{14,15} and its length is comparable to the maximal resolution of optical microscopes. The use of SIF prevents one from achieving this resolution. In this work, we show that replacing random, multilayered SIF with nanoparticle monolayers (NMLs) covalently bound to glass does not affect the optical resolution of a microscope while preserving field enhancement and lifetime decrease of SIF, thus leading to reduced photobleaching. This made it possible to observe, for the first time, single molecules in muscle. Muscle is particularly difficult to work with in the SMD regime, because concentration of actin and myosin is in mM range.¹⁶

The SMD of motor protein *in vitro* was accomplished earlier. Novel methods such as total internal reflection fluorescence (TIRF) polarization microscopy¹⁷ and defocused orientation/position imaging¹⁸ were used to achieve this feat. Earlier work showed that single molecule motion of smooth muscle myosin,^{19,20} myosin 5,^{18,21,22} myosin 6,^{23,24} kinesin,^{25,26} cytoplasmic dynein,²⁷ RNA polymerase,²⁸ ATP synthase,²⁹ and the flagellar motor³⁰ can be measured *in vitro*. The task is more formidable *in vivo*, where the concentration of proteins is greater (1-cm segment of a single muscle fiber may contain more than 10^{13} actin monomers). Recently, orientation of a single cross-bridge in rigor has been measured *in vivo*.³¹

In this work, we visualized single molecules of actin in muscle by labeling actin with phalloidin. Labeling actin with phalloidin offers the essential advantages in that the degree of labeling can be strictly controlled, and that in skeletal muscle (in contrast to cardiac muscle), only the ends of thin filaments are initially labeled.³² This is the region where actin and cross-bridges interact. Thus our data do not contain information contributed by actin in the I-bands or Z-lines, where it does not interact with cross-bridges. Additional advantages are that actin labeling does not affect enzymatic properties of muscle,^{33,34} that myofibrils are well preserved, because labeling does not require harsh conditions such as raising the temperature to label myosin light chains, and that fluorescence brightness of phalloidin increases on binding to actin,³⁴ thus increasing SNR.

Muscle was illuminated by total internal reflection, and fluorescence was detected using an electron-multiplying charge-coupled device (EMCCD). Back-thinned electron-

multiplying CCD cameras have 60% greater quantum efficiency than instruments based on photomultipliers. Wide-field TIRF illumination exploits the fact that a camera is a parallel acquisition device (as opposed to a point-by-point serial scanner), which allows light to be collected over a much longer integration time at each pixel than is possible with scanning devices. A new generation of back-thinned EMCCD has improved photosensitivity, and has a wider dynamic range. These performance characteristics enable imaging at very low light levels.³⁵ The time course of photobleaching was followed with subsecond time resolution. Myofibrils were labeled with decreasing ratios of fluorescence: nonfluorescent phalloidin ranging from 1×10^{-4} to 0.5×10^{-6} to assure that less than one actin monomer per overlap zone was fluorescent. On glass substrate, the fluorescence of the O-bands decayed in a step-wise fashion due to the discrete bleaching of a fluorophore. On NML coated glass, the fluorescence of a single actin molecule remained approximately constant over 100 sec. On the average, it decayed four to five times slower than on glass substrate. NML decreased the average amplitude weighted fluorescence lifetime 17 times, and enhanced the fluorescence intensity ten times in comparison with glass. NML decreased photobleaching because decrease in the lifetime of the fluorophore minimized the probability of oxygen attack during the time a fluorescent molecule was in the excited state, and decreased photodamage because field enhancement allowed illumination with a weaker laser beam.

2 Materials and Methods

2.1 Chemicals and Solutions

Rhodamine-phalloidin (RP) was from Molecular Probes (Eugene, Oregon). Unlabeled phalloidin (UP) was from Sigma (Saint Louis, Missouri). All other chemicals, including phosphocreatine, creatine kinase, glucose oxidase, catalase, and ATP, were from Sigma. Ethylene diamine tetraacetic acid (EDTA)-rigor solution contained 50-mM KCl, 2-mM EDTA, 1-mM DTT, and 10-mM Tris-HCl buffer pH 7.5. Ca-rigor solution contained 50-mM KCl, 4-mM MgCl_2 , 0.1-mM CaCl_2 , 1-mM dithiothreitol (DTT), and 10-mM Tris-HCl buffer pH 7.5. Contracting solution was the same as Ca-rigor, except that it contained in addition 2-mM ATP.

2.2 Preparation of Myofibrils

Muscle was first washed with cold EDTA-rigor solution for 1/2 h to avoid shortening when transferred from glycerinating solution to homogenizing solution. It was followed by extensive wash with Ca-rigor solution. Myofibrils were homogenized in Ca-rigor as described before.³⁶

2.3 Labeling and Sample Preparation

Labeling was carried out in solution. Myofibrils (1 mg/mL) were labeled for 5 min with a mixture containing 0.05 to 100-nM RP containing always 10- μM UP in Ca-rigor solution. 25 μL of labeled myofibrils were applied to number 1 cover slips (20 \times 60 mm) (Corning, New York) precleaned with 90% ethanol. A narrow channel was created by applying a thin layer of Vaseline along the edges of the cover slip. To align myofibrils as much as possible, along the long axis of a cover slip, the sample was applied by streaking the pipette

along the long axis. The sample was left for 3 min to allow myofibrils to adhere to glass. The long cover slip was covered with a small (20×20-mm) cover slip and washed with at least 5 vol of Ca-rigor solution by applying the solution to one end of the channel and absorbing with number 1 filter paper at the other.

2.4 Preparation of Nanoparticle Monolayers

All necessary glassware was soaked in a base bath overnight and washed with deionized water. A solution of 18-mg/mL silver nitrate (200 mL) was heated and stirred in a 250-mL Erlenmeyer flask at 95°C. 0.5-mL aliquots of 34-mM trisodium citrate solution were added drop-wise. The solution was stirred for 20 min and warmed to 96 to 98°C. Then five aliquots (0.7 mL each) of 34-mM trisodium citrate were added drop-wise to the reaction mixture every 15 to 20 min. Stirring was continued for 25 min until the milky yellow color remained. Then the mixture was cooled in an ice bath for 15 min. The colloids were separated by centrifugation at 3500 rpm for 6 min. The residues were collected and dissolved in 1-mM trisodium citrate. For covalent attachment of the nanoparticles to glass cover slips, the cover slips were washed with Alconox soap and rinsed with distilled water. The cover slips were soaked for 2 h in 0.1-M NaOH to activate the surface, rinsed copiously with distilled water, and soaked overnight at 80 to 90°C in a solution of 5% (v/v) aminopropyltriethoxysilane buffered with 0.1-M acetic acid (pH 5.5). The coverslips were rinsed with deionized water, air dried, and placed into a petri dish for drop coating with the sol of silver colloids. About 300 μL of the colloidal silver sol was drop coated on the desired area of the glass slide/coverslip. The excess of colloidal silver sol was rinsed with deionized water after incubation for two hours at room temperature. The glass coverslips with attached silver nanoparticles were air dried and stored in vials.

2.5 Atomic Force Microscope Imaging

Imaging was performed on the AFM Explorer ThermoMicroscope (Veeco Instruments, Incorporated, Plainview, New York) in contact scanning mode with a Non-Conductive Silicon Nitride Probe (Veeco Instruments, Incorporated). Images were acquired at a 2- to 5- $\mu\text{m}/\text{s}$ scan rate with a resolution of 300 pixels per line. Images were then processed with WSxM Version 4.0 software for 3-D structure and analyzed with the Veeco SPMLab Version 6.0.2 software for z , x , and y distance quantification.

2.6 Measuring Fluorescence Lifetimes

Fluorescence lifetimes were measured by time-domain technique using a FluoTime 200 fluorometer (PicoQuant, Incorporated, Berlin, Germany). The sample was positioned in front-face configuration inside the fluorometer chamber. Excitation was by a 475-nm laser pulsed diode, and the observation was through a monochromator at 575 nm with a supporting 550-nm-long wave pass filter. Full width at half maximum (FWHM) of pulse response function was 68 ps (measured by PicoQuant, Incorporated). Time resolution was better than 10 ps. Less than 0.5% background was detected from the

NML slide. The intensity decays were analyzed in terms of a multiexponential model using FluoFit ver4 software (PicoQuant, Incorporated).

2.7 Optical Imaging

The instrument was described before,^{37,38} except that an Olympus IX71 (Olympus, Melville, New York) was used. A Hamamatsu ImagEM CCD camera (Hamamatsu, Bridgewater, New Jersey) was mounted in the right exit port (model IX2 RSPC-2) of the microscope. The left exit port contained a confocal aperture and the avalanche photodiode, as previously described.³⁸ It was used for statistical analysis of the reduction of photobleaching. Excitation light from an expanded diode pumped solid state (DPSS) laser beam (Compass 215M, Coherent, Santa Clara, California) was coupled by the polarization-preserving-fiber to a commercial TIRF attachment (Olympus), which was mounted on the back port of the microscope. The attachment expanded the laser beam, focused it at the back focal plane of the objective, and directed it by the movable optical fiber adapter to the periphery of the objective (Olympus Apo 100×, 1.65 NA, or PlanApo 60×, 1.45 NA). Excitation light totally internally reflected at the interface and produced an evanescent wave on the aqueous side of the interface.³⁹ Exciting light was s-polarized (perpendicular to the incidence plane), giving an evanescent field similarly linearly polarized.⁴⁰ Fluorescence was excited with linearly polarized light parallel or perpendicular to the myofibrillar axis. The sample rested on a moveable piezo stage (Nano-H100, Mad City Labs, Madison, Wisconsin) controlled by a nano-drive. The fluorescent light was collected through the same objective, projected onto a tube lens and to a calcite prism (Melles Griot, Carlsbad, California), which split the fluorescent light into two orthogonally polarized components. The light was focused on the photosensitive area of the camera. The insertion of the calcite prism did alter by a few millimeters the position of the conjugate image plane, but in practice it made a negligible difference to the focus because the high magnification objective (with long back focal distance) was used.

The coupling of the DPSS laser to the TIRF module was done through polarization preserving single mode optical fibers. Those fibers have small diameters ($\sim 3 \mu\text{m}$) and are notoriously difficult to couple efficiently with the laser beam. We used a commercial fiber (kineFlex, PointSource, England) mounted into a kinematic adapter (Model KC1, Thor, Newton, New Jersey) to assure high coupling efficiency ($\sim 50\%$), i.e., $\sim 25 \text{ mW}$ of 532-nm light was launched into a TIRF module.

2.8 Spatial Sampling

The pixel size of the camera is $16 \times 16 \mu\text{m}$. For the 60× NA 1.45 objective with 532-nm illumination, the Rayleigh resolution limit is $\sim 200 \text{ nm}$. According to the Nyquist sampling theorem, the ideal spatial sampling rate should have been $200/2.3 \approx 90 \text{ nm}$. However, in our experiments the image was undersampled. The back-projected size of the pixel of the camera is $16 \mu\text{m}/60 = 267 \text{ nm}$. Therefore, the images are undersampled by a factor of $267/90 \approx 3$. For the 100× NA 1.65 objective, the back-projected size of the pixel of the camera is 160 nm, and the images are undersampled by

factor of ~ 1.8 . Undersampling allows the light to be concentrated on fewer pixels. Under the present low-light conditions, this creates a signal that has greater amplitude relative to the background noise, and therefore boosts SNR.

2.9 Choice of Sampling Time

The whole field (512×512 pixels) is collected at time intervals τ . The choice of τ is crucial in SMD. Decreasing τ increases time resolution but decreases the number of fluorescent photons detected from each half-sarcomere. Increasing τ improves SNR but decreases time resolution. We took $\tau = 100$ to 400 ms as a reasonable compromise, because the characteristic time for ATP hydrolysis by glycerinated skeletal myofibrils is ~ 0.5 sec.⁴¹ The time resolution can be increased by increasing camera gain at the expense of image quality.

2.10 Image Analysis

HCImage software (Hamamatsu) was used. Rectangular ROI was created corresponding to each O-band in a 512×512 image. The intensity measurement tool was used to measure the mean gray value of all the defined ROIs in all 500 images. ROI was 4×4 pixels (slightly smaller than a half-sarcomere). These data were saved as tabbed text files. The ASCII file was plotted in SigmaPlot (Systat, San Jose, California). The deconvolution of point spread function (PSF) was done to see if weak uniform fluorescence of unstained myofibrils was due to the spread of fluorescence. The analysis showed that it was not. The MATLAB function `deconvblind` (MathWorks Incorporated, Natick, Massachusetts) was used. It uses a maximum likelihood algorithm to iteratively optimize the PSF when deconvolving the image. The algorithm maximizes the likelihood that the resulting image, when convolved with the resulting PSF, is an instance of the blurred image, assuming Poisson noise statistics. Deconvolution made images less blurred, but the basic observation, that unstained myofibrils were fluorescent, was unchanged.

3 Results

3.1 Number of Observed Molecules

We first measured the volume of muscle sarcomere to estimate the number of observed actin molecules. Figure 1 shows AFM images of unlabeled (top) and labeled (bottom) myofibril. The AFM image reports on the resistance to stress encountered by the atomic probe. The images look different, but it is important to emphasize that the difference in AFM image does not suggest that phalloidin induces changes in the sarcomere structure. Because phalloidin binding makes the ends of thin filaments stiffer, this region of a sarcomere is more difficult for an atomic probe to deform. It is known that the pattern of phalloidin labeling changes with time. Initially only the ends of thin filaments are labeled.³² Redistribution of phalloidin to the I-band takes several hours.⁴² Myofibrils used here were observed 5 to 15 min after labeling, so only the ends of thin filaments were labeled.

The average height of 12 phalloidin-labeled myofibrils was 97 ± 4 nm (mean+SEM). The typical width and length of a sarcomere are 0.8 and 2.5 μm , respectively, so the typical volume of a half-sarcomere is ~ 0.1 $\mu\text{m}^3 = 0.1 \times 10^{-15}$ L.

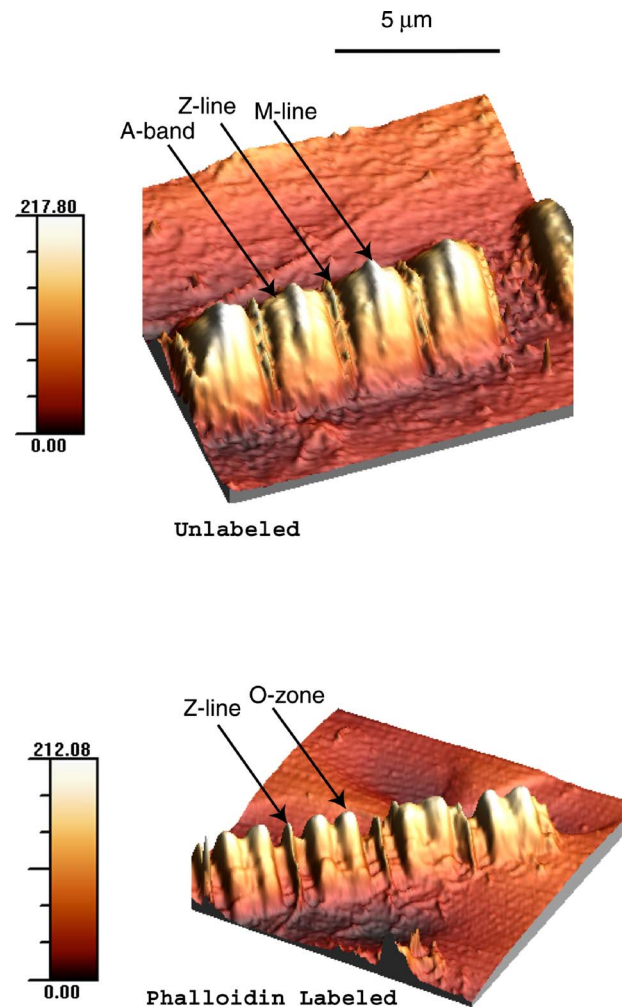


Fig. 1 AFM image of a native myofibril on glass coverslip and of a myofibril labeled with 0.1 - μM RP+ 9.9 - μM UP. The color scale bar indicates distance from coverslip in nanometers.

Since the concentration of actin in muscle is 0.6 mM,¹⁶ this volume contains on average 0.4×10^5 actin monomers.

For “heavily” labeled muscle (see Fig. 2), where 1 in 10^2 molecules are labeled, we have ~ 400 labeled actin molecules per half-sarcomere. For “lightly” labeled muscle (see Fig. 3), where 1 in 10^4 molecules are labeled, we have on average ~ 4 labeled actin molecules per half-sarcomere. For “extremely lightly” labeled muscle (see Fig. 6) where 1 in 10^5 molecules are labeled, we have on average ~ 0.4 labeled actin molecules per half-sarcomere.

3.2 Photobleaching of Heavily Labeled Myofibrils on Glass

If the concentration of the label is high, many actins carry the fluorophores. For heavily labeled myofibrils, we used 100 nM RP ($+9.9$ μM nonfluorescent label), i.e., 1 in 100 actin monomers carry fluorescent phalloidin. The number of observed actin molecules is ~ 400 per half-sarcomere. The top panel of Fig. 2 shows the time course of photobleaching of the myofibrils labeled with 100 nM RP+ 9.9 μM UP. 500 images were captured every 200 ms; but only frames 1, 50, 100, 200,

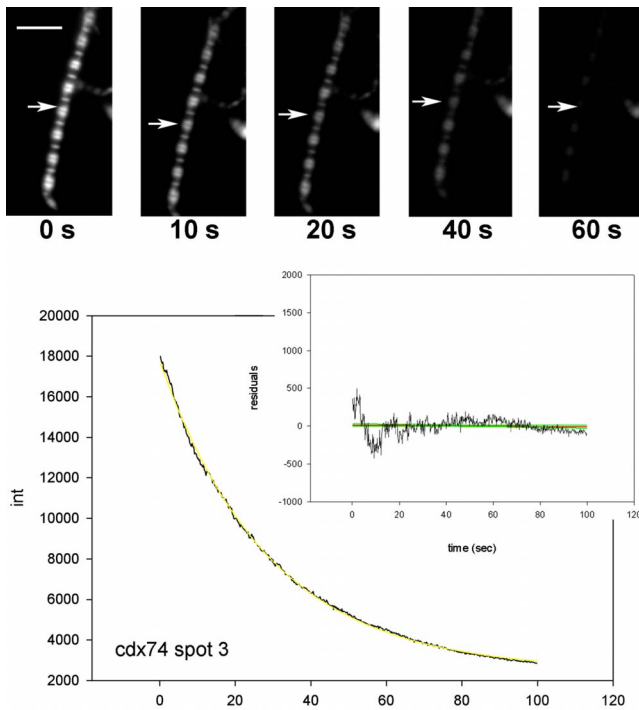


Fig. 2 The time course of photobleaching of heavily labeled rigor myofibril. Top panel: myofibril at times indicated below each frame. Exciting light polarized vertically, emitted light polarized horizontally. The bar is $5\ \mu\text{m}$. Sarcomere length= $2.6\ \mu\text{m}$. Bottom panel: the time course of photobleaching of the O-band pointed to by the arrow in the top panel (black). The least-square three-parameter exponential fit (yellow) is $y = 2469 + 15291 \exp(-6.9 \times 10^{-3} t)$. The inset is the difference between the signal and the exponential function showing that the exponential is a good fit to the data. Red is the best linear fit to residuals, and green is 95% confidence limit. Myofibril is labeled with $0.1\text{-}\mu\text{M}$ RP+ $9.9\text{-}\mu\text{M}$ UP. Myofibrils are on sapphire, viewed by $100\times$ NA= 1.65 objective. (Color online only.)

and 300 are shown. The time course of photobleaching of the O-band pointed to by the arrow in the top panel is plotted in the bottom panel of Fig. 2. The three-parameter exponential (yellow) fits the data closely. The half-time is ~ 20 sec.

It is important to point out that we measure polarized intensity of fluorescence. The sample was always illuminated with light polarized vertically relative to the laboratory frame of reference. The microscope field of view is split into two orthogonally polarized parts by the calcite prism inserted before the camera (see Sec. 2). This causes the camera to see two images simultaneously, obtained with the analyzer oriented horizontally and vertically. The myofibril shown in Fig. 2 was viewed with the analyzer oriented horizontally.

3.3 Photobleaching of Lightly Labeled Myofibrils on Glass

In contrast to smooth photobleaching of the heavily labeled O-bands, sarcomeres of lightly labeled myofibrils bleached in step-wise fashion. The example is shown in Fig. 3. For myofibrils labeled with 1-nM RP+ $10\text{-}\mu\text{M}$ UP and using the value of 0.4×10^5 actin monomers per half-sarcomere, we estimate that it contains ~ 4 molecules of phalloidin. Figure 3 shows images that were captured every 400 ms. The time course of photobleaching of the O-band pointed to by the arrow in the

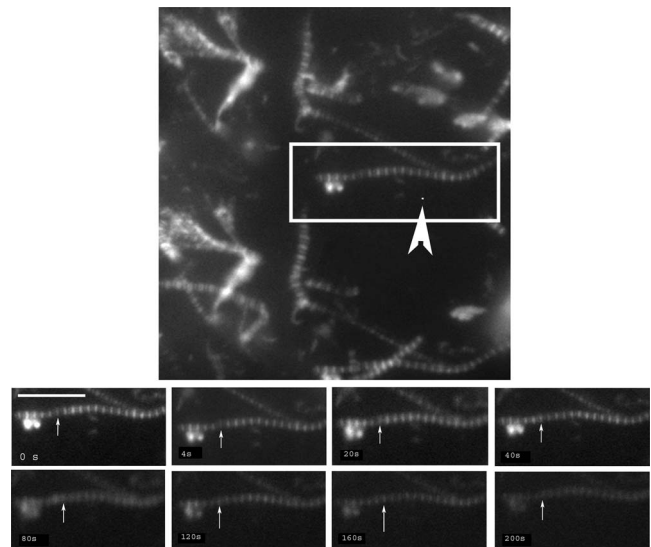


Fig. 3 The time course of photobleaching. Top panel: the whole field. Myofibril enclosed in the box was analyzed. The arrow points to the background ROI. Bottom: intensity of fluorescence of the sarcomere, pointed to by an arrow, was measured every 400 ms. The times at which images were taken after opening the shutter are shown at the bottom left. The bar is $10\ \mu\text{m}$. Sarcomere length= $2.1\ \mu\text{m}$. Myofibrils are labeled with $1\ \text{nM}$ RP+ $10\text{-}\mu\text{M}$ UP.

bottom panel of Fig. 3 after subtracting the background is plotted in Fig. 4. It suggests the presence of two discrete steps. Most of the O-bands in the top panel of Fig. 3 also bleached in step-wise fashion. However, not all of the steps were as clearly defined. We estimate that only $\sim 50\%$ of 480 spots analyzed in 12 separate experiments in which sarcomeres were not uniformly labeled bleached in a clearly defined step-wise fashion. The pattern of photobleaching varied from O-band to O-band. Even the O-bands immediately adjoining each other gave different patterns. For example, the O-band immediately to the right of the one pointed to by an arrow in Fig. 3 suggested that bleaching occurred in four steps. The fact that not all sarcomeres bleached in a step-wise fashion is perhaps due to the fact that some sarcomeres we selected for analysis were not containing fluorophores at all, but were fluorescent due to waveguide effect.

The time course of the bleaching of the background from the same sized ROI used to collect data from the O-band (pointed to by an arrowhead in the top panel of Fig. 3) is plotted as an inset to Fig. 4. It displays fluorescence equal to $\sim 60\%$ of the signal (recall that the signal is plotted after subtracting the background). However, the inset shows that the bleaching occurs smoothly. The residuals of the least-squares fit to the three-parameter exponential decay function (data not shown) suggested that the exponential is a good fit to the data. This bleaching is most likely due to residual fluorophores remaining stuck to the glass after washing. The rest of the background (~ 6000 units) is due to the autofluorescence of glass. It does not photobleach at all.

3.4 Photobleaching of Extremely Lightly Labeled Myofibrils on Glass

To image a half-sarcomere containing on average less than one fluorescent actin per half-sarcomere, we used 0.1-nM

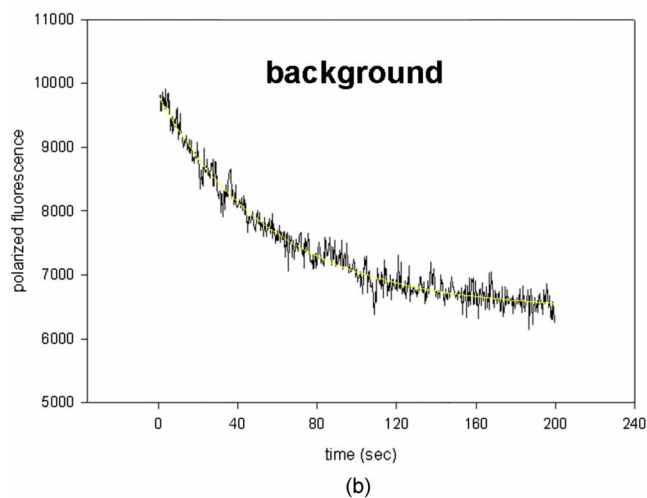
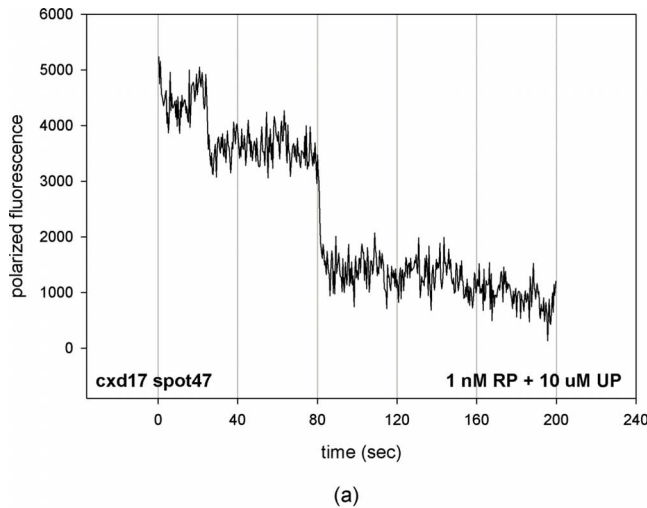


Fig. 4 (a) The time course of photobleaching of the O-band pointed to by the arrow in the bottom panel of Fig. 3, suggesting the presence of discrete steps. Other O-bands in this frame also bleached in a step-wise fashion. Signal change suggests two steps. Note that the vertical scale is the intensity **after** subtracting background. The inset shows the time course of photobleaching of an O-band labeled with 10-nM RP. (b) shows the time course of photobleaching of the background pointed to by the arrow in the top panel of Fig. 3. The least square three-parameter exponential fit (yellow) is $y=6447 + 3356 \exp(-6.90 \times 10^{-3} t)$. (Color online only.)

RP+10- μ M UP. For an estimated number of actin molecules in a half-sarcomere of 0.4×10^5 , this gives ~ 0.4 molecules of phalloidin actin in a ROI. Figure 5 shows the time course of photobleaching of the myofibrils irrigated with 0.1-nM RP +10- μ M UP. The time course of photobleaching of the O-band pointed to by the arrow in Fig. 5 is plotted in Fig. 6. It suggests the presence of a single discrete step.

3.5 Photobleaching of Heavily and Lightly Labeled Myofibrils on the Nanoparticle Monolayer

Figure 7 (top panel) shows the representative examples of images of myofibrils on glass. The images are of good quality, as evidenced by the fact that the Z-bands (pointed to by the arrowheads) and the H-zones (pointed to by the arrows) are well resolved. The bottom panel of Fig. 7 shows representa-

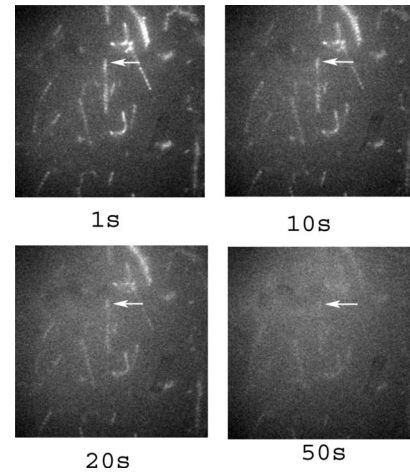


Fig. 5 The time course of photobleaching of myofibrils labeled with 0.1-nM RP+10- μ M UP. Intensity of fluorescence of the sarcomere pointed to by an arrow was measured every 100 ms. The times at which images were taken after opening the shutter are shown below each frame. Sarcomere length=2.0 μ m.

tive examples of myofibrils on the NML. The comparison with images on glass shows that image quality remains equally good, as evidenced by the resolution of the Z-bands (arrowheads) and the H-zones (arrows). The intensity is larger in the bottom panels than in the top because colloids increase brightness an average of ten times. This is not reflected in brightness of images because camera gain was adjusted automatically. We did not observe any photobleaching within 100 sec. The same was true for lightly labeled myofibrils (1-nM RP+10- μ M UP).

3.6 Photobleaching of Extremely Lightly Labeled Myofibrils on the Nanoparticle Monolayers

Nanoparticle monolayers reduced photobleaching principally through the reduction of fluorescent lifetime (see Discussion Sec. 4). The top panel of Fig. 8 shows the image of a myo-

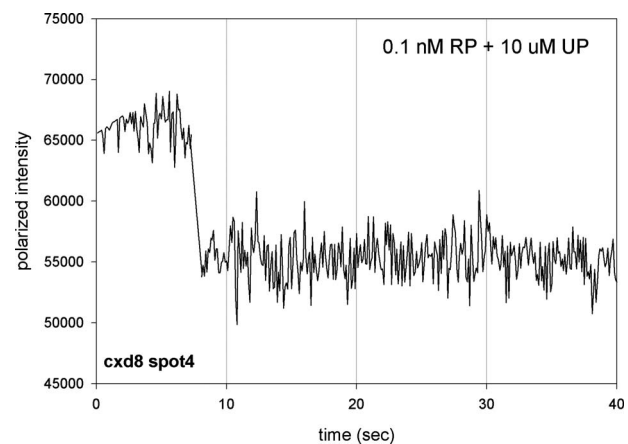


Fig. 6 The time course of photobleaching of an O-band pointed to by an arrow in Fig. 5. Signal change (black) suggests a single step. The least square three-parameter exponential fit (yellow) is $y=35061 + 33277 \exp(-4.42 \times 10^{-3} t)$. Myofibrils were labeled with 0.1-nM RP+10- μ M UP. The background has been subtracted.

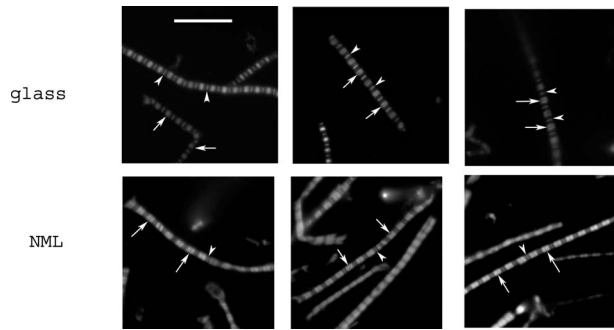


Fig. 7 Representative images of myofibrils on glass (top panels) and on NML (bottom panels). Arrowheads point to the Z-lines and arrows point to the H-zones. Myofibrils are labeled with 0.1- μ M rhodamine phalloidin +9.9- μ M unlabeled phalloidin. Bar is 10 μ m. TIRF excitation. The fact that myofibrils are on average 10 times brighter on NML than on glass is not well illustrated in this figure, because the gain of the camera adjusted itself automatically.

fibril labeled with 0.1-nM RP+10- μ M UP on NML. It is important to point out that NML signal from myofibril was enhanced approximately ten times in comparison with signal on glass (see next). The increase of brightness reduced photodamage because it allowed illumination with a weaker laser light. The bottom panel compares signal from a sarcomere containing \sim 1 fluorophore (red) with a signal from the background (black). The transient is caused by “blinking” of silver particles on glass. Metallic silver nanoparticles display curious “blinking,” even in the absence of the fluorophores.^{43,44} Fortunately, blinking is rare. In one half-sarcomere, we have detected on average only three to four events during 100 sec.

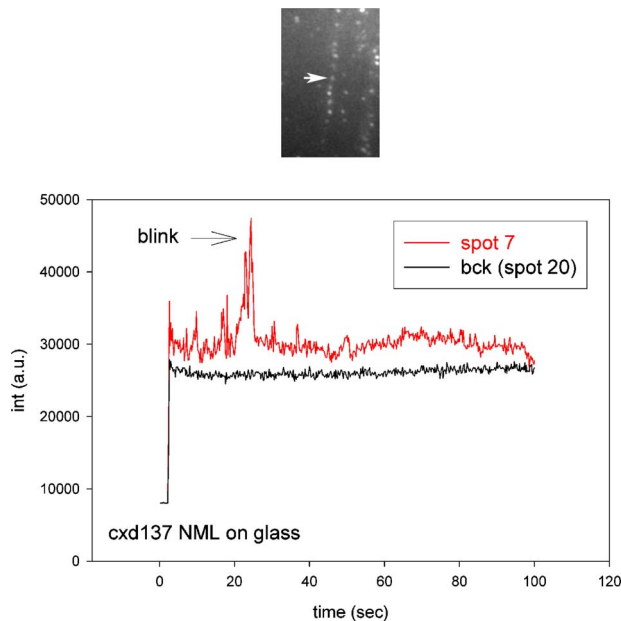


Fig. 8 The time course of photobleaching of myofibrils labeled with 0.1-nM RP+10- μ M UP. The intensity of fluorescence of the sarcomere pointed to by an arrow in the top panel was measured every 100 ms. The horizontal scale is the times at which images were taken after opening the shutter. Note that NML increased the brightness ten fold. The data were taken through 1 OD filter. (Color online only.)

3.7 Rate of Photobleaching

To obtain an average reduction of photobleaching, we measured signal by avalanche photodiode. We used NA=1.45, 60 \times objective and 8- μ m confocal aperture. This makes the depth of the detection volume (equal to the depth of the evanescent wave) \sim 100 nm. The x - y dimension of the detection volume is equal to the diameter of the confocal aperture divided by the magnification of the objective. With an 8- μ m aperture and 60 \times objective, it is smaller than the diffraction limit of the objective i.e., the diameter of the volume is 0.25 μ m,⁴⁵ giving the detection volume of 18×10^{-18} L. Actin concentration in muscle (0.6 mM) implies that there are \sim 6800 actin protomers in this volume. The ratio of fluorescent phalloidin to nonfluorescent phalloidin was fixed at 1:1000, suggesting that the signal was contributed by approximately seven to eight actin molecules. Figure 9(a) shows that the NML enhanced intensity of fluorescence ten fold in comparison with glass. Figure 9(b) compares the rate of photobleaching of the myofibrillar overlap zone on glass (green) and NML (red). NML signal from myofibril was enhanced ten times in comparison with signal on glass, so signal on NML was divided by this factor to make intensities at time 0 the same. The half-time of decay on glass and on large colloids was increased approximately four times, but in 12 experiments this time increased on average from 14 ± 4 to 69 ± 25 sec (approximately four to five times).

3.8 Decrease of Fluorescent Lifetime

Figure 10 shows that the enhancement of intensity and decrease of photobleaching is indeed due to decrease of lifetime. NML augmented the fast decay of fluorescein-labeled myofibrils (arrow). The fluorescence decay (black) after a laser flash (gray) is best fitted (black) by the two exponentials with lifetimes $\tau_1=0.92$ and $\tau_2=4.02$ ns, with the relative contributions to the total amplitude of 48.5 and 51.5%, respectively. The average amplitude weighted lifetime was 2.52 ns. The arrows point to the fast decay of fluorescence. NML significantly decreased the lifetime signal. It is now best fitted (white) by three exponentials with lifetimes $\tau_1=1.181$, $\tau_2=3.421$, and $\tau_3=0.066$ ns with the relative contributions to the total amplitude of 2.0, 1.8, and 96.2%, respectively. The average amplitude weighted lifetime was 0.150 ns. The arrows point to the fast decay of fluorescence. The average decrease of lifetime was 17 times, but it is worth pointing out that, whereas there was no ultrafast component of decay of myofibrils on glass, such a component constituted 96% of a signal on NML.

4 Discussion

By observing muscle on glass with sensitive EMCCD, it was possible, for the first time, to visualize single actin molecules in muscle. Discrete photobleaching observed on glass is a useful indicator of a single molecule regime, but it is an obstacle when making kinetic measurements, because photobleaching steps obscure intensity fluctuations due to molecular motions. For example, in muscle, intensity fluctuates because of rotations of myosin molecules. Changes of intensity due to photobleaching are superimposed on rotational signals, making rotations impossible to detect. By observing

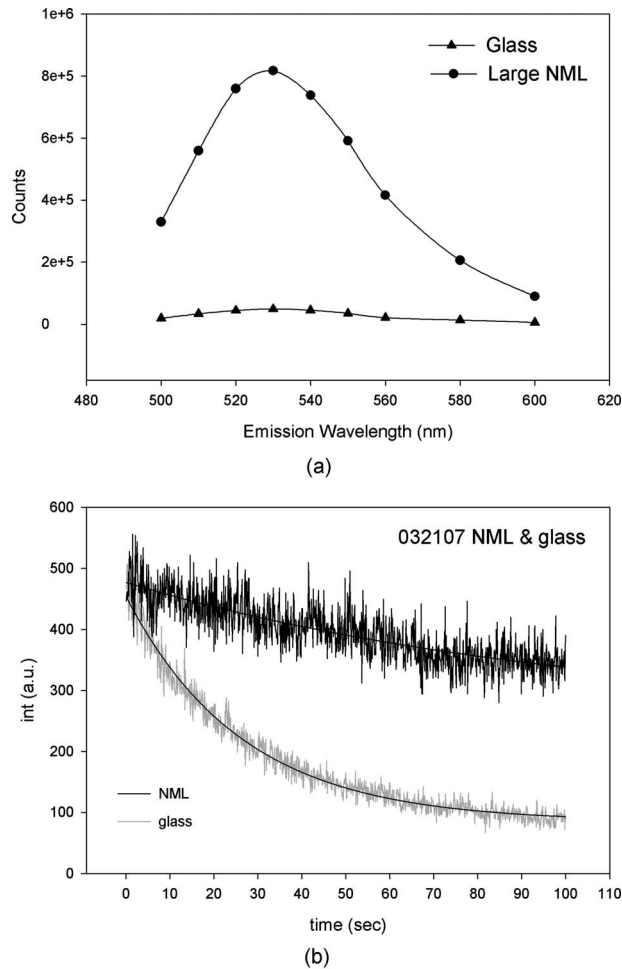


Fig. 9 (a) Comparison of spectra of myofibrils (1 mg/mL) labeled with 0.1- μM fluorescein-phalloidin on a glass coverslip coated with monolayers containing colloids (circles). The spectra were measured at a 45 deg angle in a Varian Eclipse spectrofluorometer. Excitation wavelength was 475 nm. The spectrum of glass alone is shown as triangles. The spectrum of a colloid monolayer in the absence of muscle was comparable to glass alone. (b) Comparison of the rate of photobleaching of the myofibrillar overlap zone on glass and NML. The overlap zone of a myofibril was viewed through a 133-nm back-projected confocal aperture. Gray—myofibrils on glass. Decay of fluorescence is best fitted by three-parameter exponential fit $y=84.5 + 369 \exp(-3.8 \times 10^{-3} t)$ (black curve). Black—myofibrils on NML. Decay of fluorescence is best fitted by three-parameter exponential fit $y=255 + 221 \exp(-9.9 \times 10^{-4} t)$ (black curve). Intensity is measured in counts-per-100 ms bin. Colloid enhanced the signal ~ 10 times, so the signal on NML was divided by this factor to make intensities at time 0 the same. Myofibrils (1 mg/mL) were labeled with 0.01- μM rhodamine-phalloidin + 9.99- μM unlabeled phalloidin. TIRF illumination, sarcomere viewed through an 8- μm aperture. NA=1.45 objective.

muscle on nanoparticle monolayers, it was possible to image single molecules for at least 100 sec without photobleaching them.

Observing single molecules in muscle is particularly important, because the molecules that are responsible for contraction, myosin cross-bridges, act asynchronously. Probing single molecules avoids the averaging inherent in studying large assemblies of molecules. Further, observing single mol-

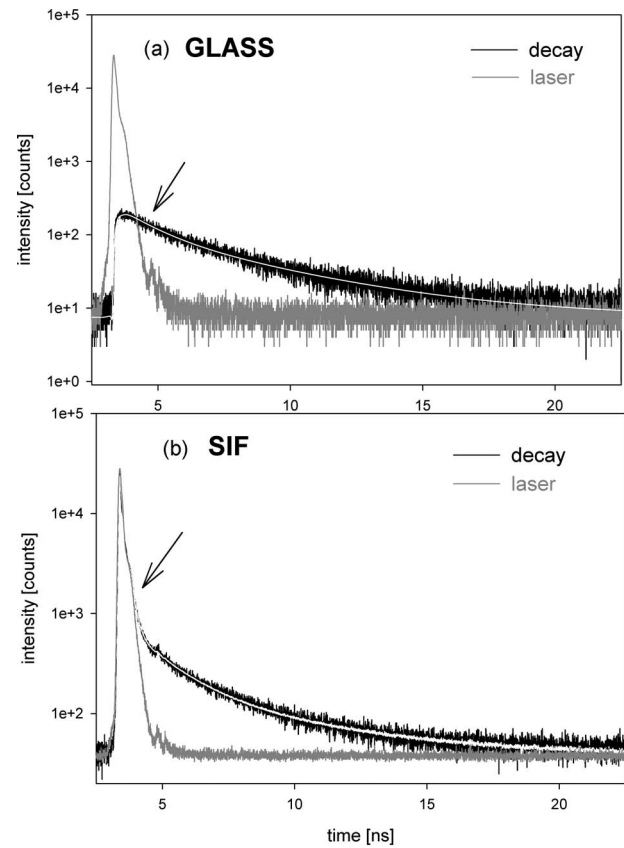


Fig. 10 Decrease of fluorescent lifetime by NML. (a) Lifetime signal from myofibrils on glass (black). The signal is best fitted (white line) by the two exponentials with lifetimes $\tau_1=0.92$ and $\tau_2=4.02$ ns, with the relative contributions to the total amplitude of 48.5 and 51.5%. The average amplitude weighted lifetime was 2.52 ns. The arrow points to the fast decay of fluorescence. The gray signal is the exciting pulse from the diode laser. The bottom inset is the residual fit to all 9567 data points. (b) Lifetime signal from myofibrils on glass coated with a SIF monolayer (black) is best fitted (white line) by three exponentials with lifetimes $\tau_1=1.181$, $\tau_2=3.421$, and $\tau_3=0.066$ ns, with the relative contributions to the total amplitude of 2.0, 1.8, and 96.2%, respectively. The average amplitude weighted lifetime was 0.150 ns. The arrow points to the fast decay of fluorescence. The gray signal is the exciting pulse. The bottom inset is the residual fit to all 5308 data points. 1-mg/mL myofibrils were labeled with 0.1- μM rhodamine-phalloidin.

ecules *in situ* avoids possible alteration of cross-bridge kinetics by the regular arrangement of actin and myosin in arrays of filaments, by molecular crowding and the dependence of kinetic rates on position within a sarcomere. Even though it is possible to avoid asynchrony by applying transients in length or ATP concentration and thus forcing thousands of cross-bridges to act as one,^{46,47} there are differences between isometric and transient experiments. In the isometric case, cross-bridges act against steady maximum force, whereas during transients they act initially, acting against no load.

The presence of nanoparticles has three effects. 1. In a close proximity, below ~ 20 Å, there is a strong quenching of fluorescence. The excitation energy is being damped to the metal in a nonradiative way. This does not affect fluorescence from myofibrils, because they rise at least 150 nm above the surface of the nanoparticles.³ 2. An electric field of excitation

light is significantly altered near nanoparticles. Locally, this field can be very strong. The fluorophores in this region are exposed to a strong excitation, which results in an increased brightness. The enhanced local field is responsible also for surface-enhanced Raman scattering (SERS). 3. The interaction of excited molecules with metallic nanoparticles results in a rapid emission of a photon to the far field. This effect (known also as a radiative decay engineering) increases a radiative rate (Γ) of fluorophore deactivation.⁴⁸ In this case, the quantum efficiency increases, and the lifetime decreases. Decrease of lifetime is sufficient proof that the radiative rate is increased. Indeed, in conventional fluorescence, the changes in quantum efficiency (Q) always occur by modulation of the nonradiative rate constant (k_{nr}), be it by solvent relaxation, nonradiative decay, quenching by the solvent, or transfer of the energy to an acceptor. The radiative rate constant Γ remains constant. Thus a decrease in k_{nr} always causes an increase of fluorescence lifetime, $\tau=1/(\Gamma+k_{nr})$. In contrast, the proximity of fluorophores to metallic particles provides an opportunity to modify radiative rate Γ . For example, suppose the metallic particles result in a γ -fold increase in the radiative decay rate to $\Gamma_{mod}=\gamma\Gamma$. The lifetime $\tau=1/(\gamma\Gamma+k_{nr})$ becomes shorter. Our experiments confirmed that lifetime indeed decreased (Fig. 10). Increase in Γ causes fluorescence to become brighter, because quantum yield now becomes $Q=\gamma\Gamma/(\gamma\Gamma+k_{nr})$, i.e., it becomes closer to the maximum value of 1. (In our case, Q is near 1 anyway (because we are using rhodamine); this increase is not very significant.) However, the main beneficial effect is a decrease of lifetime. This causes significant decrease of bleaching, because the fluorophore spends less time in the excited state, and leads to a more effective excitation rate, because fluorophores are more often excited.

To strengthen the conclusion that the step-wise decrease in signal results from photobleaching of a single molecule of phalloidin, we need to estimate the number of fluorescent photons given off by one rhodamine molecule before bleaching. To do so, we need to convert the gray values of EMCCD to the number of photons. We took advantage of our ability to direct the signal either to the EMCCD camera or to the avalanche photodiode (see Materials and Methods in Sec. 2). For the data shown as inset in Fig. 4, we determined that the number of photons corresponding to the signal at time 0 was ~ 4000 . The corresponding gray level of the camera was $\sim 20,000$. From the figure, we estimate that the change of gray level associated with one step is 2000, i.e., we get ~ 400 photons/step. A step lasted ~ 40 sec, i.e., we observed $\sim 16,000$ photons from a fluorophore before it photobleached. (The duration of the first step is underestimated, because it takes a few seconds to focus the image. During this time, photobleaching is already in progress.) The geometrical collection efficiency of the instrument is $\sim 2\%$,³⁸ thus a fluorophore emitted a total of 0.8×10^6 photons before irreversible bleaching. This is consistent with the known photostability of rhodamine.⁴⁹

5 Conclusions

On a glass substrate, molecules photobleach rapidly. If many molecules are observed, photobleaching is smooth (Fig. 2). If a few molecules (Fig. 4) or one molecule (Fig. 6) is observed,

photobleaching is step-wise, reflecting individual bleaching events. Nanoparticle monolayers, in contrast to multilayers, do not decrease the quality of images of myofibrils (Fig. 7). Monolayers increase the brightness [Fig. 9(a)], thus reducing photodamage because it allows illumination with weaker laser light. The significant decrease of photobleaching [Figs. 8 and 9(b)] is caused by a reduction of fluorescent lifetime (Fig. 10). Reduction of photobleaching and photodamage makes single molecule detection in tissue less problematic than detection on glass.

Acknowledgment

This work was supported by grant number RO1 AR048622 (to Borejdo) from NIH.

References

1. E. Betzig, R. J. Chichester, F. Lanni, and D. L. Taylor, "Near field fluorescence imaging of cytoskeletal actin," *Bioimaging* **1**, 129–133 (1993).
2. E. Betzig, G. H. Patterson, R. Sougrat, O. W. Lindwasser, S. Olenych, J. S. Bonifacino, M. W. Davidson, J. Lippincott-Schwartz, and H. F. Hess, "Imaging intracellular fluorescent proteins at nanometer resolution," *Science* **313**(5793), 1642–1645 (2006).
3. P. Muthu, I. Gryczynski, Z. Gryczynski, J. Talent, I. Akopova, K. Jain, and J. Borejdo, "Decreasing photobleaching by silver island films: application to muscle," *Anal. Biochem.* **366**(2), 228–236 (2007).
4. D. A. Weitz, S. Garoff, C. D. Anson, and T. J. Gramila, "Fluorescent lifetimes of molecules on silver-island films," *Opt. Lett.* **7**, 89–91 (1982).
5. A. Leitner, M. E. Lippitch, S. Draxler, M. Riegler, and F. R. Aussenegg, "Fluorescence properties of dyes absorbed to silver islands, investigated by picosecond techniques," *Appl. Phys. B* **36**, 105–109 (1985).
6. I. Gryczynski, J. Malicka, Y. Shen, Z. Gryczynski, and J. R. Lakowicz, "Multiphoton excitation of fluorescence near metallic particles: Enhanced and localized excitation," *J. Phys. Chem. B* **106**, 2191–2195 (2002).
7. B. P. Maliwal, J. Malicka, I. Gryczynski, Z. Gryczynski, and J. R. Lakowicz, "Fluorescence properties of labeled proteins near silver colloid surfaces," *Biopolymers* **70**(4), 585–594 (2003).
8. C. D. Geddes, H. Cao, I. Gryczynski, Z. Gryczynski, and J. R. Lakowicz, "Metal-enhanced fluorescence (MEF) due to silver colloid on a planar surface: Potential applications of indocyanine green to in vivo imaging," *J. Phys. Chem. A* **107**, 3443–3449 (2003).
9. J. Malicka, I. Gryczynski, and J. R. Lakowicz, "DNA hybridization assays using metal-enhanced fluorescence," *Biochem. Biophys. Res. Commun.* **306**(1), 213–218 (2003).
10. J. Malicka, I. Gryczynski, J. Fang, and J. R. Lakowicz, "Photostability of Cy3 and Cy5-labeled DNA in the presence of metallic silver particles," *J. Fluoresc.* **12**, 439–447 (2002).
11. S. Hayashi, "Spectroscopy of gap modes in metal particle-surface systems," in *Topics in Applied Physics, Near Field Optics and Surface Plasmon Polaritons*, S. Kawata, Ed., Vol. 81, pp. 71–95, Springer-Verlag, Berlin (2001).
12. J. R. Lakowicz, Y. Shen, S. D'Auria, J. Malicka, J. Fang, Z. Gryczynski, and I. Gryczynski, "Radiative decay engineering 2. Effects of silver island films on fluorescence intensity, lifetimes, and resonance energy transfer," *Anal. Biochem.* **301**, 261–277 (2002).
13. P. Muthu, I. Gryczynski, Z. Gryczynski, J. M. Talent, I. Akopova, and J. Borejdo, "Decreasing photobleaching by silver nanoparticles on metal surfaces: application to muscle myofibrils," *J. Biomed. Opt.* **13**, 014033 (2008).
14. A. M. Gordon, A. F. Huxley, and F. J. Julian, "The variation in isometric tension with sarcomere length in vertebrate muscle fibres," *J. Physiol. (London)* **184**(1), 170–192 (1966).
15. A. M. Gordon, A. F. Huxley, and F. J. Julian, "Tension development in highly stretched vertebrate muscle fibres," *J. Physiol. (London)* **184**(1), 143–169 (1966).
16. C. R. Bagshaw, *Muscle Contraction*, Chapman and Hall, London (1982).

17. J. N. Forkey, M. E. Quinlan, and Y. E. Goldman, "Measurement of single macromolecule orientation by total internal reflection fluorescence polarization microscopy," *Biophys. J.* **89**(2), 1261–1271 (2005).
18. E. Toprak, J. Enderlein, S. Syed, S. A. McKinney, R. G. Petschek, T. Ha, Y. E. Goldman, and P. R. Selvin, "Defocused orientation and position imaging (DOPI) of myosin V," *Proc. Natl. Acad. Sci. U.S.A.* **103**(17), 6495–6499 (2006).
19. D. M. Warshaw, E. Hayes, D. Gaffney, A. M. Lauzon, J. Wu, G. Kennedy, K. Trybus, S. Lowey, and C. Berger, "Myosin conformational states determined by single fluorophore polarization," *Proc. Natl. Acad. Sci. U.S.A.* **95**(14), 8034–8039 (1998).
20. M. E. Quinlan, J. N. Forkey, and Y. E. Goldman, "Orientation of the myosin light chain region by single molecule total internal reflection fluorescence polarization microscopy," *Biophys. J.* **89**(2), 1132–1142 (2005).
21. J. N. Forkey, M. E. Quinlan, M. A. Shaw, J. E. Corrie, and Y. E. Goldman, "Three-dimensional structural dynamics of myosin V by single-molecule fluorescence polarization," *Nature (London)* **422**(6930), 399–404 (2003).
22. A. Yildiz, J. N. Forkey, S. A. McKinney, T. Ha, Y. E. Goldman, and P. R. Selvin, "Myosin V walks hand-over-hand: single fluorophore imaging with 1.5-nm localization," *Science* **300**(5628), 2061–2065 (2003).
23. H. Park, B. Ramamurthy, M. Travaglia, D. Safer, L. Q. Chen, C. Franzini-Armstrong, P. R. Selvin, and H. L. Sweeney, "Full-length myosin VI dimerizes and moves processively along actin filaments upon monomer clustering," *Mol. Cell* **21**(3), 331–336 (2006).
24. H. Park, A. Li, L. Q. Chen, A. Houdusse, P. R. Selvin, and H. L. Sweeney, "The unique insert at the end of the myosin VI motor is the sole determinant of directionality," *Proc. Natl. Acad. Sci. U.S.A.* **104**(3), 778–783 (2007).
25. M. E. Quinlan, J. N. Forkey, and Y. E. Goldman, "Kinesin-ADP: whole lotta shakin' goin' on," *Nat. Struct. Biol.* **8**(6), 478–480 (2001).
26. A. Yildiz and P. R. Selvin, "Kinesin: walking, crawling or sliding along?," *Trends Cell Biol.* **15**(2), 112–120 (2005).
27. S. Toba, T. M. Watanabe, L. Yamaguchi-Okimoto, Y. Y. Toyoshima, and H. Higuchi, "Overlapping hand-over-hand mechanism of single molecular motility of cytoplasmic dynein," *Proc. Natl. Acad. Sci. U.S.A.* **103**(15), 5741–5745 (2006).
28. E. A. Abbondanzieri, W. J. Greenleaf, J. W. Shaevitz, R. Landick, and S. M. Block, "Direct observation of base-pair stepping by RNA polymerase," *Nature (London)* **438**(7067), 460–465 (2005).
29. H. Ueno, T. Suzuki, K. Kinosita, Jr., and M. Yoshida, "ATP-driven stepwise rotation of FoF1-ATP synthase," *Proc. Natl. Acad. Sci. U.S.A.* **102**(5), 1333–1338 (2005).
30. Y. Sowa, A. D. Rowe, M. C. Leake, T. Yakushi, M. Homma, A. Ishijima, and R. M. Berry, "Direct observation of steps in rotation of the bacterial flagellar motor," *Nature (London)* **437**(7060), 916–919 (2005).
31. T. P. Burghardt, K. Ajtai, D. K. Chan, M. F. Halstead, J. Li, and Y. Zheng, "GFP tagged regulatory light chain monitors single myosin lever-arm orientation in a muscle fiber," *Biophys. J.* **18**, 18 (2007).
32. D. Szczesna and S. S. Lehrer, "The binding of fluorescent phallox-
ins to actin in myofibrils," *J. Muscle Res. Cell Motil.* **14**(6), 594–597 (1993).
33. A. E. Bukatina, F. Fuchs, and S. C. Watkins, "A study on the mechanism of phalloidin-induced tension changes in skinned rabbit psoas muscle fibres," *J. Muscle Res. Cell Motil.* **17**(3), 365–371 (1996).
34. E. Prochniewicz-Nakayama, T. Yanagida, and F. Oosawa, "Studies on conformation of F-actin in muscle fibers in the relaxed state, rigor, and during contraction using fluorescent phalloidin," *J. Cell Biol.* **97**, 1663–1667 (1983).
35. K. Garsha, "Spectral methods for biological analysis," *Photonics Spectra* **41**(8), 53–58 (2007).
36. J. Borejdo, O. Assulin, T. Ando, and S. Putnam, "Cross-bridge orientation in skeletal muscle measured by linear dichroism of an extrinsic chromophore," *J. Mol. Biol.* **158**, 391–414 (1982).
37. J. Borejdo, J. Talent, I. Akopova, and T. P. Burghardt, "Rotations of a few cross-bridges in muscle by confocal total internal reflection microscopy," *Biochim. Biophys. Acta* **1763**, 137–140 (2006).
38. J. Borejdo, P. Muthu, J. Talent, I. Akopova, and T. P. Burghardt, "Rotation of actin monomers during isometric contraction of skeletal muscle," *J. Biomed. Opt.* **12**, 014013 (2007).
39. D. Axelrod, "Total internal reflection fluorescence microscopy," *Methods Cell Biol.* **30**, 245–270 (1989).
40. T. P. Burghardt and N. L. Thompson, "Effect of planar dielectric interfaces on fluorescence emission and detection. Evanescent excitation with high-aperture collection," *Biophys. J.* **46**, 729–737 (1984).
41. E. J. Potma, I. A. van Graas, and G. J. Stienen, "Effects of pH on myofibrillar ATPase activity in fast and slow skeletal muscle fibers of the rabbit," *Biophys. J.* **67**(6), 2404–2410 (1994).
42. X. Ao and S. S. Lehrer, "Phalloidin unzips nebulin from thin filaments in skeletal myofibrils," *J. Cell. Sci.* **108**(Pt. 11), 3397–3403 (1995).
43. L. A. Peyser, A. E. Vinson, A. P. Bartko, and R. M. Dickson, "Photoactivated fluorescence from individual silver nanoclusters," *Science* **291**(5501), 103–106 (2001).
44. C. D. Geddes, A. Parfenov, I. Gryczynski, and J. R. Lakowicz, "Luminescent blinking from silver nanostructures," *J. Phys. Chem.* **107**, 9989–9993 (2003).
45. J. Borejdo, Z. Gryczynski, N. Calander, P. Muthu, and I. Gryczynski, "Application of surface plasmon coupled emission to study of muscle," *Biophys. J.* **91**, 2626–2635 (2006).
46. S. C. Hopkins, C. Sabido-David, J. E. Corrie, M. Irving, and Y. E. Goldman, "Fluorescence polarization transients from rhodamine isomers on the myosin regulatory light chain in skeletal muscle fibers," *Biophys. J.* **74**(6), 3093–3110 (1998).
47. J. Borejdo, A. Shepard, D. Dumka, I. Akopova, J. Talent, A. Malka, and T. P. Burghardt, "Changes in orientation of actin during contraction of muscle," *Biophys. J.* **86**, 2308–2317 (2004).
48. J. R. Lakowicz, J. Malicka, I. Gryczynski, Z. Gryczynski, and C. Geddes, "Radiative decay engineering: the role of photonic mode density in biotechnology," *J. Phys. D* **36**, R240–R249 (2003).
49. C. Eggeling, J. Widengren, R. Rigler, and C. A. M. Seidel, "Photobleaching of fluorescent dyes under conditions used for single-molecule detection: evidence of two-step photolysis," *Anal. Chem.* **70**, 2651–2659 (1998).